Hydrogen trapping in an API 5L X60 steel

P. Castaño Rivera [a,*], V.P. Ramunni [b], P. Bruzzoni [c]

[a] Instituto de Tecnología Jorge Sabato, Av. General Paz 1499, B1650KNA, San Martín, Prov. de Buenos Aires, Argentina
[b] CONICET, Av. Rivadavia 1917, CPC1033AAJ, CABA, Argentina
[c] Comisión Nacional de Energía Atómica, Av. del Libertador 8250 (1429), CABA, Argentina

ARTICLE INFO

ABSTRACT

Electrochemical hydrogen permeation tests were performed on an API 5L X60 steel to study trapping and diffusion properties in the as-received (AR) and in a cold-rolled (CR) state, at 30, 50 and 70 °C. Hydrogen trapping was characterized by assuming saturable traps in local equilibrium. Binding energies (ΔG) and trap densities (N) were determined by fitting a trapping theoretical model to experimental data. Both conditions AR and CR present a high density of weak traps $|\Delta G| < 35$ kJ/mol, namely $N = 1.4 \times 10^{-5}$ and 7.9×10^{-4} mol/cm^3 respectively. Strong trapping sites were detected ($-72 < \Delta G < -57$ kJ/mol) and their densities increased markedly after cold-rolling.

1. Introduction

The steels specified in the API standard (American Petroleum Institute), are mainly used in natural gas and petroleum pipelines, and are generally characterized by their good mechanical strength, weldability and fracture toughness among other properties [1]. However, these materials are susceptible to some type of hydrogen damage. A well known type of damage is the hydrogen assisted cracking. This phenomenon, which has been studied extensively [2–5] is related to hydrogen diffusion. Ferritic and martensitic steels have microstructural imperfections called traps which hold hydrogen in the atomic form. A remarkable observation is that the H diffusion process is delayed by the presence of traps. These traps have been related to microstructural features such as dislocations, interfaces, vacancies, impurity atoms, microvoids or any other lattice defect [4]. The effect of cold-working on the hydrogen trapping characteristics of iron and steels has been studied extensively; the pioneering works appeared in the 1950's. Darken and Smith [6] suggested that in steels subjected to a cold-rolling process, the H diffusion can be affected by the presence of traps which are created during the plastic deformation of the material. Bath and Lloyd [7] studied different steels (with different carbon percentage), which were cold-drawn to different reduction degrees. The experimental setup was a hollow steel cylinder in which hydrogen was introduced by cathodic charging on the external surface. After permeating through the steel wall, hydrogen was collected in the internal hole and measured by a volumetric method. Their results indicated that the H permeation rate at room temperature increases with time and finally reached a steady state value. The time to reach the steady state increased markedly as the degree of plastic deformation increased. They observed also that the steady state permeation rate decreased markedly with increasing plastic deformation. However, they were suspicious on the latter result and argued that either the different rates of hydrogen pickup (cathodic charging) or insufficient time to attain a true steady state might have influenced the results. In fact, later results [8] showed a moderate influence of the degree of cold-work on the steady state H permeation rate in a 0.48%C steel. In additional experiments [7], the amount of hydrogen absorbed after 24 h cathodic charging ("H saturation") was measured by hot extraction in vacuum. Bath and Lloyd [7] observed that the H saturation became is higher as the degree of cold-work increased. This confirmed the hypothesis that plastic strain created sites that capture hydrogen. In other classical work Keeler and Davis [9] showed, via H$_2$-equilibration with a Sieverts-like technique, that the amount of H absorbed by a SAE 1020 steel (0.17 %C) at 250–550 °C steel was influenced by a cold-rolling process performed on this material. Thus, the amount of H occluded in the plastically strained steel after equilibration at 250 °C was about 100 times higher than the amount of H occluded in the not strained steel. Keeler and Davis [9] also observed that the density of the 1020 steel decreased as the degree of cold-work increased up to 60% reduction in thickness. They attributed the decrease in density to the formation of microvoids as result from imperfect plastic flow of the ferrite about inclusions or other phases during cold-rolling. The increase in the hydrogen absorption capacity was related to these microvoids. However, additionally to the microvoids, they proposed a second type of trap which was eliminated by annealing.

* Corresponding author. Tel.: +54 005411 67727785; fax: +54 005411 67727362.
E-mail addresses: patricariva@gmail.com, pcastanio@cnea.gov.ar (P. Castaño Rivera), vpram@cnea.gov.ar (V.P. Ramunni), bruzzoni@cnea.gov.ar (P. Bruzzoni).

Numerous works along a period of six decades dealt with the creation of hydrogen traps in iron and iron base alloys as a result of plastic deformation. Just a selected group of papers concerning the behavior of hydrogen in pure iron or low alloy steels is cited here. The most frequently applied techniques were hydrogen permeation [10–12] and thermal desorption spectroscopy [13,14]. As a result of these investigations, different microstructural defects in the deformed material have been associated with hydrogen traps. Dislocations are naturally the first candidates [12–14]; however, the density of hydrogen traps calculated from the density of dislocations is not equal to the trap density inferred from permeation measurements [10]; moreover, trap density decreases markedly after annealing at low temperatures at which the dislocations should be stable [10]. Microvoids caused by cold-work are other possible type of traps [9,10,13]. However, the results of permeation tests are not consistent with this type of non-saturable traps [15]. Nagumo et al. [14] proposed that vacancy clusters produced by cold-work are important hydrogen traps. In the case of low alloy steels, additional trap types such as interfaces with second phase particles are considered [12]. With reference to the hydrogen exchange rate between trap sites and normal interstitial lattice sites (NILS), usually the local equilibrium hypothesis [16] is assumed. This implies a high NILS-trap exchange rate in comparison with the diffusion rate. However, thermal desorption results are better described as limited by an activated release rate from the traps [13]. This brief literature review is intended to show that there is still a controversy on the true nature of the hydrogen traps in deformed iron and steel, and on the way these traps exchange hydrogen with NILS.

As result of the delay in the H diffusion because of the presence of lattice imperfections, the apparent diffusion coefficient (D_{app}) is lower than the diffusion coefficient in a perfect body centered cubic lattice of iron (D_L). The magnitude of the H diffusion delay depends on the strength of the trap, i.e. the free energy of trapping (ΔG) and the trap density (N), i.e. the number of trap sites per unit volume. Both parameters, ΔG and N, can be calculated through the theoretical fit of experimental H permeation curves of the H flux J_H [mol H/(cm^2 s)] versus time t [s]. In the present work, i_H vs. t curves were obtained from H permeation tests with electrochemical detection, i_H [A/cm^2] being the current density due to the oxidation of H at the exit side of the permeation membrane, i.e. the faradic equivalent of J_H. In the present work, a numerical method has been used to calculate theoretical permeation transients. This method, which is described in the Appendix, solves the differential equations described in the McNabb and Foster work [17]. These authors assume the presence of one type of trapping site and they define two kinetic constants for the H trapping and H release named k and p respectively. Also, they consider that traps are saturable, i.e. each trap can retain only one H atom; in this way the H saturation concentration is equal to the density of traps. In 1970, Oriani [16] simplified the model proposed by McNabb and Foster, assuming that the trapping and liberation velocities are high enough in comparison with the velocities involved in the diffusion process. This implies a local equilibrium condition between H in traps with the diffusing H. The numerical resolution for the MacNabb and Foster diffusion equations has been developed for several authors [15,18,19]. In these literature works, the permeation transients were numerically simulated by fixing the values of the parameters D, k, p and N, where D is the diffusion coefficient. Johnson and Lin [15] simulated the H permeation transients to study the nature of traps in cold-rolled iron. Ramunni et al. [19] obtained the trapping parameters for three different morphologies of the cementite Fe$_3$C, generated by an adequate scheme of thermal treatments.

In the present work the diffusion and trapping parameters of an API 5L X60 steel were obtained from the data of hydrogen permeation experiments with gas phase charging and electrochemical detection. Two different sample conditions were studied: as-received from the manufacturer (AR), and cold- rolled with a thickness reduction of ca. 2% (CR). The H trapping energy (ΔG) and the trap density (N) of the API 5L X60 steel were calculated from the H permeation data based on the theoretical considerations described in the Appendix of the present work, under the assumption of saturable traps in local equilibrium. As shown in Section A.7 of the Appendix, trapping energy values in the range of -35 to -70 kJ mol^{-1} are considered as "strong" or high energy traps, and their particular N and ΔG values have been directly assessed from the permeation data as fitting parameters; traps with $|\Delta G| \leqslant 35$ kJ mol^{-1} are considered as "weak" and their effect is only reflected in the value of the apparent diffusion coefficient D_{app}, which is reduced in comparison with the diffusion coefficient of a trap free lattice of bcc iron D_L.

2. Materials and methods

The material employed in this study is an API 5L X60 steel taken from a seamless pipe. The chemical composition is shown in Table 1.

A previous work [20] reported the microstructural characterization and the study of the non-metallic inclusions of this material in the as-received (AR) condition. The metallographic observation indicated that the microstructure of the API 5L X60 contains equi-axed ferrite grains and carbides mainly located in the grain boundaries, which is typical of tempered martensite. The average grain size is estimated as 4 μm and the mean size of the observed cementite particles is ca. 0.3 μm. Analysis of the local chemical composition by Energy Dispersive X-ray Spectroscopy microanalysis (EDAX) revealed few non-metallic inclusions containing varying amounts of Ca, S, Al and Ti.

From this material a parallelepiped of ca. 3.5 mm thickness was constructed, which was subjected to plastic deformation by cold-rolling in consecutive steps. The reduction in thickness (e) was 2.1 ± 0.3%, and it was calculated according to:

$$e = (L_i - L_f)/L_i \tag{1}$$

where L_i is the parallelepiped thickness before cold-rolling and L_f is the parallelepiped thickness after the last step of rolling. From the rolled parallelepiped a disk was made with a thickness of 3.39 mm and a diameter of 35 mm. Also, a disk with a thickness of 1.57 mm and a diameter of 35 mm was cut directly from the AR material. These disks were used in the electrochemical permeation tests as the permeation membranes representative of the CR and AR conditions, respectively. Prior to the tests, both disk faces (entry and exit surface of the permeation membrane) were ground with SiC up to #600 grit and then electropolished in a mixture of 10% HClO$_4$ and 90% butyl cellosolve at a temperature below 5 °C under a potential difference of 36 V. The objective of electropolishing is to eliminate a layer of 10 μm of material from each membrane face, which is the estimated thickness of the deformed layer created by mechanical polishing. Then, a palladium film about 10 nm thick was electrochemically deposited on both membrane entry and exit surfaces. The deposition cell was equipped with a Pd/PdH reference electrode and a Pt counter electrode, and it was filled with ca. 300 ml of electrolyte, which was an aqueous solution of 0.1 M NaOH. The electrolyte was continuously deaereated by nitrogen bubbling. Prior to the deposition, the permeation membrane was etched in HCl 50%, rinsed with water and immediately subjected to cathodic polarization in the electrochemical cell at a constant current density of -0.1 mA cm^{-2}. The cathodic treatment continued until the typical potential of H$_2$ evolution on the steel (-0.970 mV vs. normal hydrogen electrode, NHE) was reached. The deposition was started by introducing in the cell 7 ml of an aqueous solution of [Pd(NO$_2$)$_4$]Na$_2$

Table 1
Chemical composition of the API 5L X60 steel (weight %).

C	Mn	Si	Cr	Mo	V	Cu	Ni	Al	P	S	Ti	Nb
0.14	1.04	0.25	0.07	0.08	0.03	0.03	0.05	0.026	0.014	0.011	0.015	0.001

which contained 0.004 g/ml of Pd while keeping the current density at −0.1 mA cm^{-2}. The deposition time was 40 min. As a last step the Pd-coated membranes were degassed in an oven at 110 °C for 16 h.

The H permeation tests were carried out using gas phase charging and electrochemical detection. Gas phase charging ensures a constant and reliable chemical potential of hydrogen at the input surface [21]. The electrochemical detection technique was according to Devanathan and Stachurski [22] in an experimental arrangement similar to that outlined in reference [8]. This arrangement consists of two compartments (input cell and detection cell) separated by the steel permeation membrane which has an exposed area of 1.9 cm^2 on both their entry and exit surfaces. Gas phase charging was achieved by circulating H$_2$ (g) (99.999%) at p_{H_2}=1 bar through the input cell. The Pd film at the entry surface allows reaching equilibrium between the gas phase and the metal phase according to Sieverts' law [21]. The detection cell included a Pd/PdH reference electrode and a platinum wire as counter electrode. It contained a 0.1 M NaOH solution which was continuously deaerated with nitrogen. The exit surface of the metallic membrane was polarized at +200 mV with respect to NHE. The H flux at the exit surface was measured as its faradic equivalent i_H[A/cm^2]=$i − i_{bg}$, where i_{bg} is a background current density, mainly due to residual corrosion of the steel. The i_H values were recorded as a function of time t [s]. Permeation buildup or decay transients were obtained by circulating either H$_2$ (g) or purified air, respectively, through the input cell. The tests were performed consecutively at 30, 50 and 70 °C. At 30 °C, two successive sequences of permeation buildup and decay transients were performed in order to detect the possible presence of high energy traps.

The values of the diffusion and trapping parameters were obtained by fitting calculated hydrogen permeation transients to the experimental transients. Unlike the approach by Ramunni et al. [19], the model and software employed in the present work to calculate the permeation transients is restricted to the case of local equilibrium. Hydrogen traps are classified according to their free energy of trapping ΔG in weak traps with $|\Delta G| \leqslant 35$ kJ mol^{-1} and strong traps with $-70 < \Delta G/$kJ mol$^{-1} < -35$. A maximum of two types of strong traps is considered. The resulting fitting parameters are the apparent diffusion coefficient D_{app} and the densities and energies of the strong traps ΔG_1, N_1, ΔG_2 and N_2. The effect of the weak traps was reflected in the value of D_{app}. This method is described with more detail in the Appendix.

For the representation of the experimental and calculated permeation transients, the net H current density (i_H) and the time (t) were normalized with respect the membrane thickness (L), i.e. $i_H \times L$ vs. t/L^2.

3. Results and discussion

In the present work it is considered that the values of N and ΔG should be independent of the test temperature, because the traps, i.e. the nature and density of the metallurgical defects, is not expected to change at the test temperatures (30–70 °C). Thus, the best set of fitting parameters was selected by attempting a compromise between the goodness of the fit and the physical consistency of the results. Instead of directly using the optimal set of parameters (from the point of view of the mean quadratic deviation) for each test temperature, these values were varied slightly in order to achieve a unique value of trap density, independent

of the test temperature. In this way, the deviation between calculated and experimental data increased slightly, up to 0.1 in percentage units.
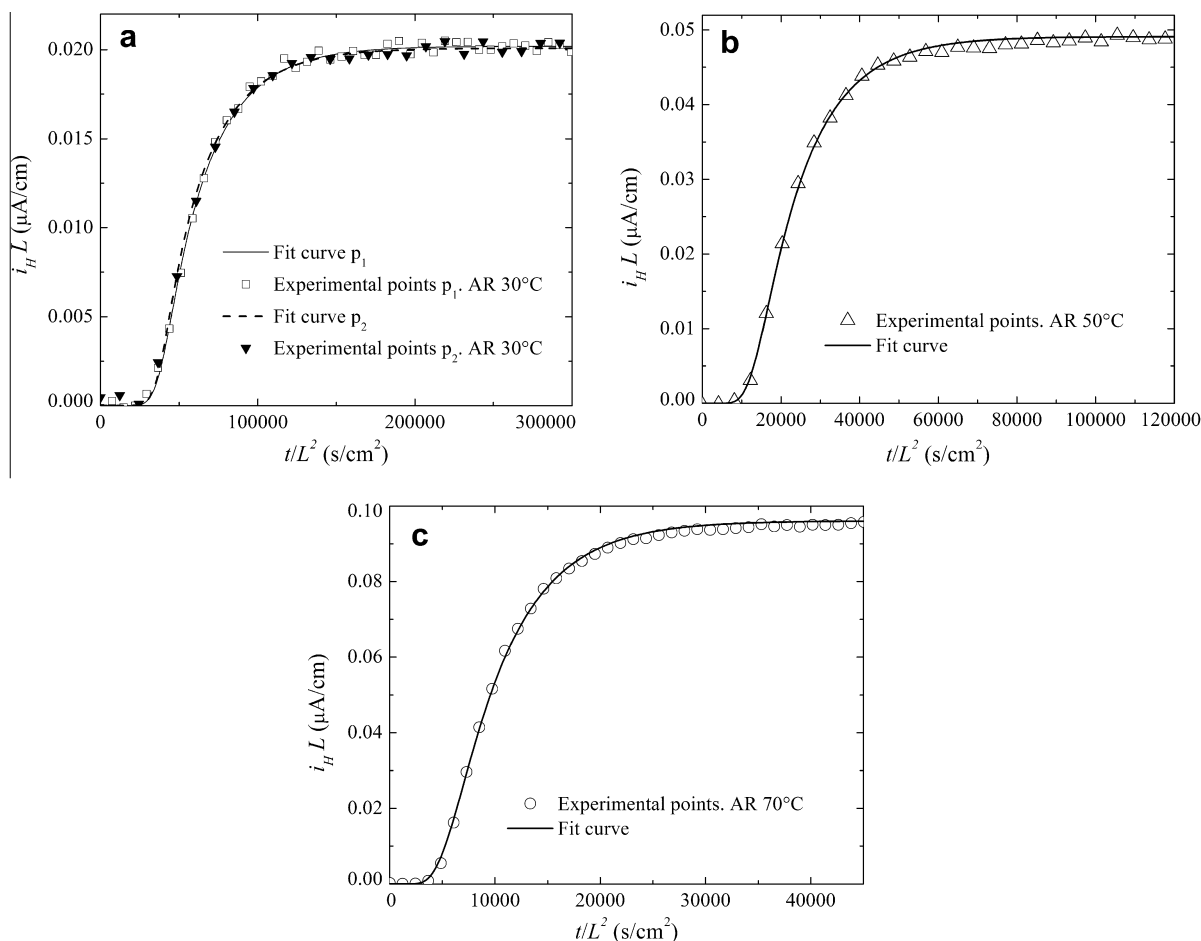
3.1. As-received condition

In the case of the AR condition it was observed that a satisfactory fit could be achieved by assuming the existence of only one type of strong traps. The experimental buildup transients are represented in Fig. 1, together with the theoretical ones identified as *fitted curve*. The selected set of parameters for the AR condition obtained from the buildup transients at 30, 50 and 70 °C is reported in Table 2. Table 2 also presents the mean quadratic deviation (expressed as percentage with respect to the steady state current density) of the fitted transients.

The first buildup transient at 30 °C corresponds to the material degassed in oven at 110 °C prior to the permeation test, which is identified in this work as *oven degassed*. The other buildup transients correspond to the material degassed in the permeation cell at the test temperature, or *cell degassed*. Thus, the trap occupancy at the beginning of the first transient at 30 °C is a priori different from that of the second transient at 30 °C. However, for the AR condition the first and second buildup transients at 30 °C look very similar, suggesting that the presence of high energy traps that retain hydrogen after cell degassing at 30 °C is not significant. Concerning the results at 30 °C, it seems reasonable to assume that the *weak traps* are completely empty either in the cell degassed or in the oven degassed condition; then, for the analysis of the first and second buildup transients at 30 °C, it is assumed that the density of weak traps is the same in both cases. Since the presence of weak traps only influences the parameter D_{app}, the fitting job is performed with the restriction that D_{app} is the same for the first and second buildup transients at 30 °C. Instead, the parameters of the *strong traps* N and ΔG were allowed to vary, in order to optimize the fit. As shown in Table 2, N obtained for the first transient at 30 °C resulted slightly higher than that observed in the others transients. Fitting of the buildup transients at the test temperatures of 50 °C and 70 °C was carried out by varying D_{app}, N and ΔG with the restriction of physical consistency discussed above.

Table 2 shows that the density of the strong traps is $N = 8 \times 10^{-9}$ mol cm^{-3} and their energy ΔG ranges from −58.3 kJ mol^{-1} to −58.6 kJ mol^{-1}, i.e. practically independent of the test temperature. The present results shows that very high energy traps (say $|\Delta G| > 60$ kJ mol^{-1}) are barely detectable in the AR condition of the API 5L X60 steel.

The decay permeation transients of the AR condition were not subjected to a fitting procedure as the buildup transients were. Instead, theoretical permeation decay transients were calculated using the parameter set obtained from the corresponding buildup transients (Table 2). Fig. 2 shows the experimental permeation decay transients and the corresponding calculated curve that is named *Theoretical curve*. The first and second decay transients at 30 °C are not expected to differ, because when they are initiated all traps should have the same occupancy in both cases. Consequently, the parameter set used to calculate the decay transients at 30 °C was that of the *second* buildup transient at 30 °C.

In this way, i.e. by simulating decay transients with the parameters of the buildup transients, it was checked whether the model described in the Appendix was able to describe the system under

Fig. 1. Experimental points and fit curves of the buildup transients for the API 5L X60 steel in the as-received (AR) condition: (a) 30 °C first transient (p_1) and second transient (p_2); (b) 50 °C; (c) 70 °C.

Table 2
Diffusion and trapping parameters of the API 5L X60 steel in the as received (AR) condition. Deviation of the fitted buildup transients and of the calculated decay transients.

Temperature (°C)	D_{app} (cm²/s)	i_{ss} (A/cm²)	ΔG (kJ/mol)	N (mol/cm³)	Deviation (%)	
					Buildup	Decay
30	3.47×10^{-6}	1.29×10^{-7}	-58.00	9.26×10^{-9}	1.25	2.49[a]
30	3.47×10^{-6}	1.28×10^{-7}	-58.60	8.00×10^{-9}	1.38	2.35
50	8.37×10^{-6}	3.13×10^{-7}	-58.02	8.00×10^{-9}	0.94	2.13
70	1.97×10^{-5}	6.12×10^{-7}	-58.32	8.00×10^{-9}	0.68	1.52

[a] Parameters of the second buildup transient at 30 °C were used.

changing experimental conditions. The deviation of the calculated points with respect to the experimental ones in the case of the decay transients was evaluated and reported in the last column of Table 2. Since the decay transient parameters are not optimized by a least squares fitting procedure, the agreement between experiment and model decreases. Anyway, the obtained deviation values, in the range of 1.5–2.5%, are considered as quite satisfactory.

3.2. Cold-rolled condition

The experimental buildup transients corresponding to the steel in the CR condition are shown in Fig. 3. From the comparison of the normalized time scales of Figs. 1 and 3 it is clear that the development of the permeation transient is retarded in the cold-rolled condition with respect to the as-received condition. This delay is expected because of the creation of traps by cold-rolling. The

remarkable fact is that this effect is very important even at this low level (~2%) of plastic strain.

As in the case of the steel in the AR condition, the optimized diffusion parameters for the CR state were obtained by fitting calculated buildup permeation transients to the experimental ones. Though, for the cold-rolled steel, considering only one type of strong trap was insufficient to achieve a good fit. Then, two types of strong traps were assumed with trap densities and energies N_1, N_2, ΔG_1 and ΔG_2 respectively. The buildup permeation transients calculated with the fitting parameters and named *Fitted curve* are in excellent agreement with the experimental data, as is shown in Fig. 3. Trapping and diffusion parameters of the API 5L X60 steel in the CR state are reported in Table 3.

As shown in Fig. 3(a), first and second buildup transients at 30 °C are notably different for the CR membrane. This observation is contrary to the results reported by Kumnick and Johnson [11] for
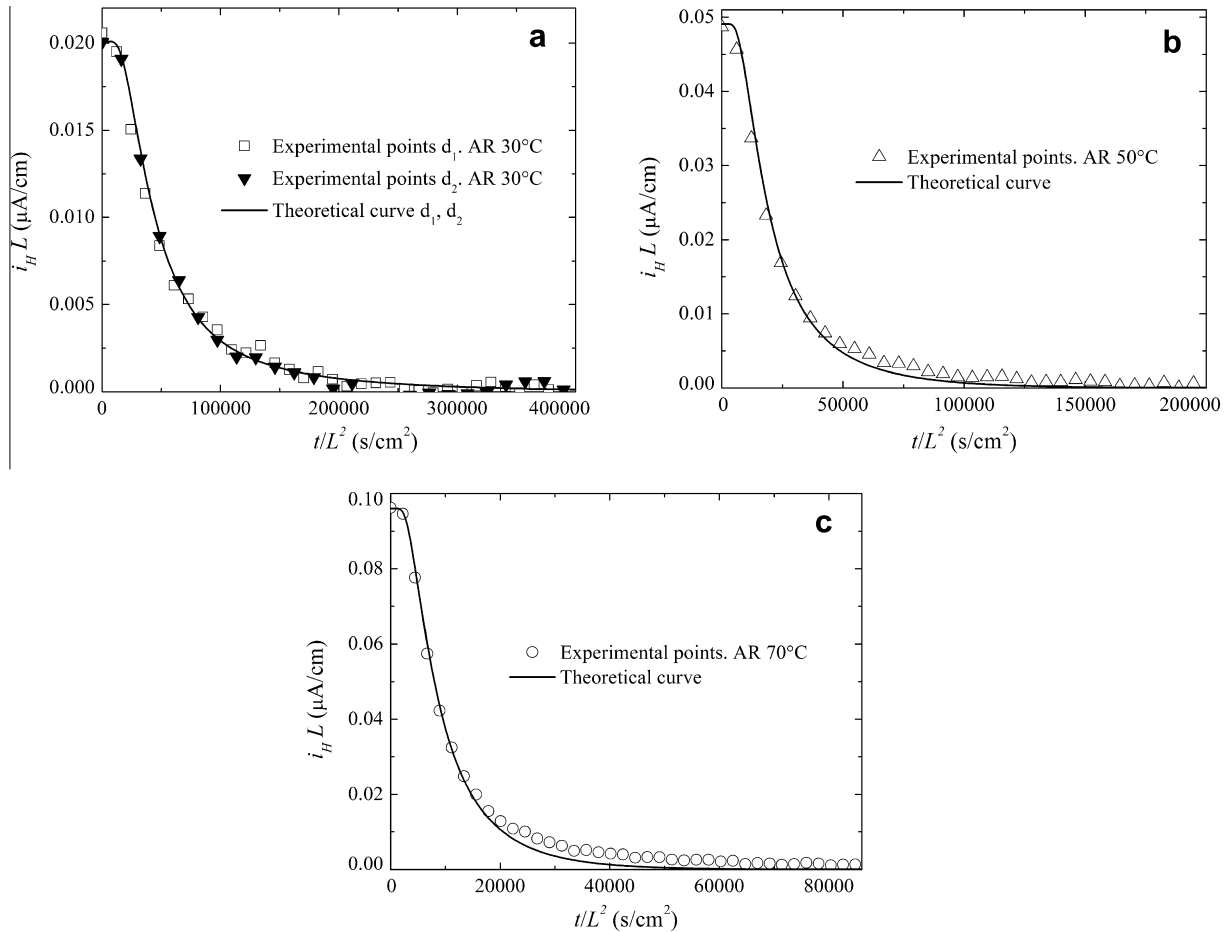
Fig. 2. Experimental points and theoretical curves of the decay transients the API 5L X60 steel in the as-received (AR) condition: (a) 30 °C first transient (d$_1$) and second transient (d$_2$); (b) 50 °C; (c) 70 °C.

pure iron. The first buildup transient at 30 °C corresponds to the *oven degassed* material. The other buildup transients correspond to the *cell degassed* material. At 30 °C and for the CR condition, the permeation buildup transient of the *oven degassed* material presents a considerable delay with respect to the permeation buildup transient of the *cell degassed* material. This delay, which was not observed in the case of the AR condition, it is attributed to the presence of very high energy traps that are emptied in the oven but not in the cell. This hypothesis is in agreement with the values of the fitting parameters N_1, N_2, ΔG_1 and ΔG_2 at 30 °C. The density of type 1 traps N_1 increases from $\sim 1.1 \times 10^{-7}$ in the *cell degassed* material to $\sim 1.8 \times 10^{-7}$ mol/cm^3 in the *oven degassed* material, and the density of type 2 traps N_2 increases respectively from $\sim 2.2 \times 10^{-8}$ to $\sim 3.1 \times 10^{-8}$ mol/cm^3. Also, the values of $|\Delta G_1|$ and $|\Delta G_2|$ for the *oven degassed* material are higher than those of the *cell degassed* material in an amount of *ca.* 3 and 12 kJ mol^{-1} respectively.

In comparison with the AR condition, the CR condition shows a marked increase in the strong trap density. In fact, the overall (type 1 + type 2) strong trap density in the CR condition is 1.2×10^{-7} mol cm, practically independent of temperature (see Table 3). This figure, corresponding to a strain $e \approx 2\%$, is 15 times higher than that of the unstrained steel. Thus, the first effect of the plastic deformation on the H diffusion and trapping behavior is a marked 2increase in the strong trap density.

The values of the trap density, N_1 and N_2, do not depend markedly on temperature. However, the absolute values of the trapping energies of the CR condition $|\Delta G_1|$ and $|\Delta G_2|$ increase moderately with temperature. This behavior is interpreted as follows: it was demonstrated above, that the CR condition presents a population of high energy traps that remain occupied during *cell degassing* at 30 °C, but are emptied by *oven degassing* at 110 °C. It is likely that an increasing fraction of this trap population will release hydrogen in the cell at increasing degassing temperatures, 50 and 70 °C. This fraction of high energy traps will be empty at the beginning of the subsequent buildup transient. This would lead to an increase in the observed average trap energy at increasing temperatures.

From the inspection of Tables 2 and 3, it can be concluded that the microstructural changes produced during cold-rolling affect the hydrogen trapping characteristics of the API 5L X60 steel and this is manifested in: (*i*) an increment of the density of weak traps reflected in a decrease of the fitting parameter D_{app} by a factor of ~ 3.2 to 4.0, (*ii*) an increment of the density of type 1 traps N_1 ($|\Delta G_1| \sim 57$–61 kJ/mol), which is 0.8×10^{-9} mol/cm^3 in the AR condition, and is increased by a factor of ~ 12 in the CR state, (*iii*) the creation of high energy type 2 traps ($|\Delta G_2| \sim 64$–73 kJ/mol), with N_2 in the range of 1.6×10^{-8} to 2.2×10^{-8} mol/cm^3; (*iv*)1 the appearance of even higher energy traps ($|\Delta G| \sim 75$ kJ/mol and $N \sim 1 \times 10^{-8}$ mol cm^{-3}) which are emptied only after oven degassing.

The fitting procedure was not carried out for the permeation decay transients corresponding to the CR state. Similar to the AR case, the theoretical decay transients were calculated using the diffusion and trapping parameters obtained from the buildup transients at the same test temperature. For the calculation of the simulated first and second decay transients at the test temperature of 30 °C,
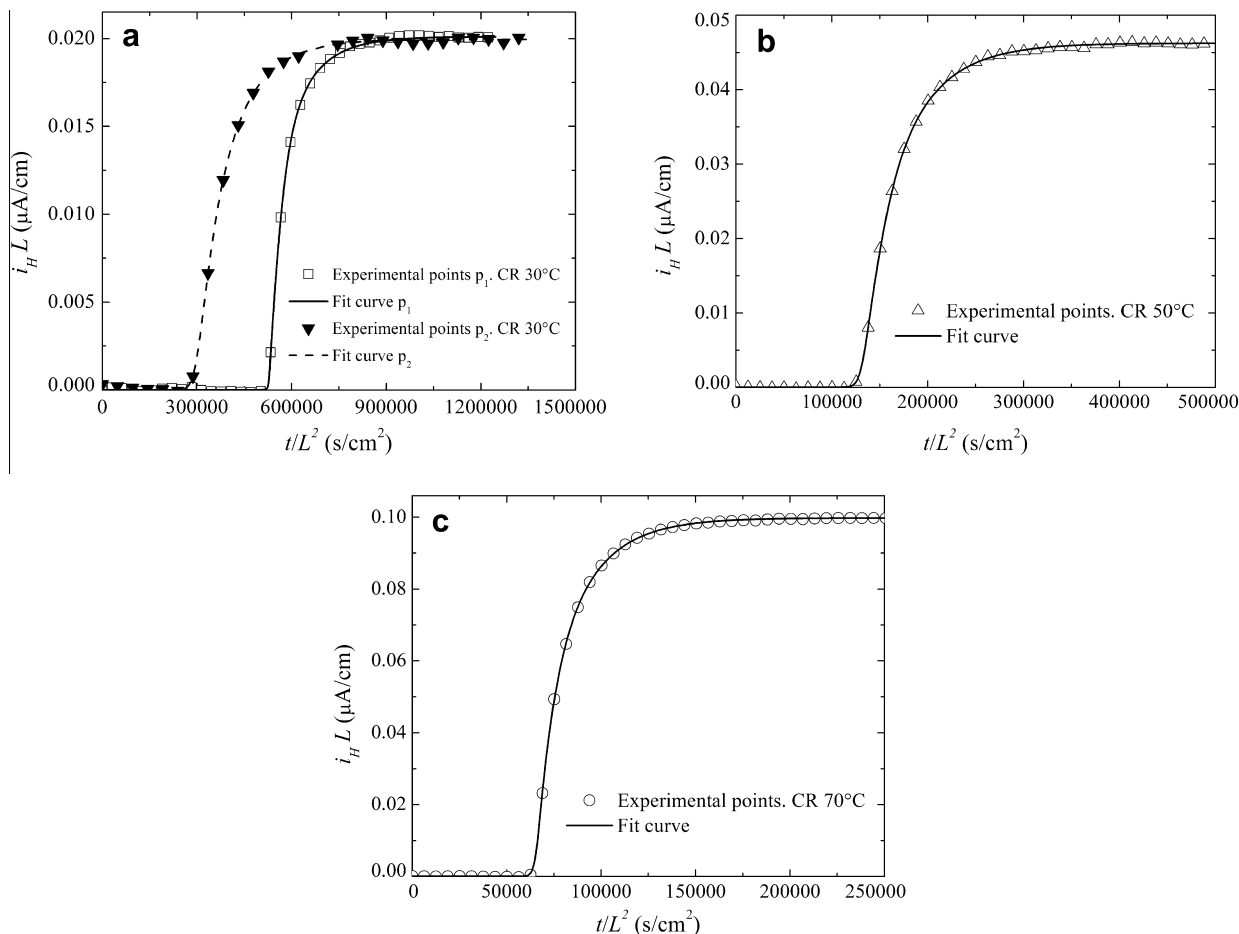
Fig. 3. Experimental points and fit curves of the buildup transients for the API 5L X60 steel in the cold-rolled (CR) condition: (a) 30 °C first transient (p_1) and second transient (p_2); (b) 50 °C; (c) 70 °C.

Table 3
Diffusion and trapping parameters of the API 5L X60 steel in the cold-rolled (CR) condition. Deviation of the fitted buildup transients and of the calculated decay transients.

Temperature (°C)	D_{app} (cm²/s)	i_{ss} (A/cm²)	ΔG_1 (kJ/mol)	N_1 (mol/cm³)	ΔG_2 (kJ/mol)	N_2 (mol/cm³)	Deviation (%)	
							Buildup	Decay
30	1.15×10^{-6}	5.93×10^{-8}	−60.38	1.79×10^{-7}	−75.86	3.14×10^{-8}	0.49	2.37[a]
30	1.10×10^{-6}	5.88×10^{-8}	−57.26	1.06×10^{-7}	−64.01	2.16×10^{-8}	0.61	2.20
50	2.46×10^{-6}	1.36×10^{-7}	−59.33	1.03×10^{-7}	−68.00	1.66×10^{-8}	0.34	0.95
70	4.99×10^{-6}	2.94×10^{-7}	−61.35	9.89×10^{-8}	−71.53	1.95×10^{-8}	0.15	1.12

[a] Parameters of the second buildup transient at 30 °C.

the parameters of the second buildup transient at 30 °C were employed, which are representative of the *cell degassed* state. The mean quadratic deviation of the calculated permeation decay transients with respect to the experimental decay transients of the CR condition is reported in the last column of Table 3. This deviation ranges from 1 to 2.5%.

In Fig. 4 the experimental permeation decay transients are plotted together with the simulated ones as described above and named as *Theoretical curve*. The coincidence, as judged from Fig. 4 and from the deviation values, is satisfactory.

3.3. Steady state permeation

The steady state H current density (i_{ss}) as a function of the temperature is practically the same for both AR and CR conditions, when it is normalized with respect the membrane thickness L (Tables 2 and 3). The independency of the steady state H flux in relation with the plastic deformation has been reported for iron of different purities [21,23]. A low alloy steel with 0.48%C and a microstructure of ferrite + pearlite showed no change of $i_{ss} \times L$ after cold-rolling to 15% reduction in thickness; however, with 70% reduction in thickness $i_{ss} \times L$ was reduced *ca.* 2.5 times [8]. The fact that the present API 5L X60 steel does not show a dependence of $i_{ss} \times L$ on strain may be due to a combination of low carbon content (0.14 wt.%) and low strain (~2%). The hydrogen permeation coefficient (Φ) was calculated from $i_{ss} \times L$ according to Eq. (A.5) that has been taken from reference [8]:
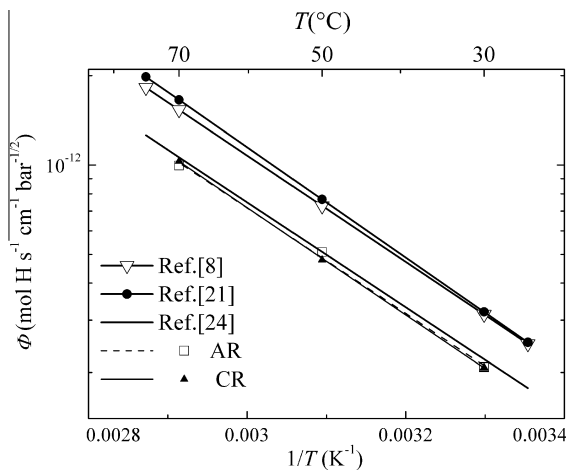
$$\Phi = \frac{i_{ss}L}{F\sqrt{p_{H_2}}}$$

(2)

where F is the Faraday constant and $p_{H_2} = 1$ bar is the H partial pressure at the input cell. Fig. 5 is an Arrhenius type plot that shows the Φ values for the AR and CR conditions, together with literature values corresponding to pure iron (Φ_{Fe}) [21,23,24] for
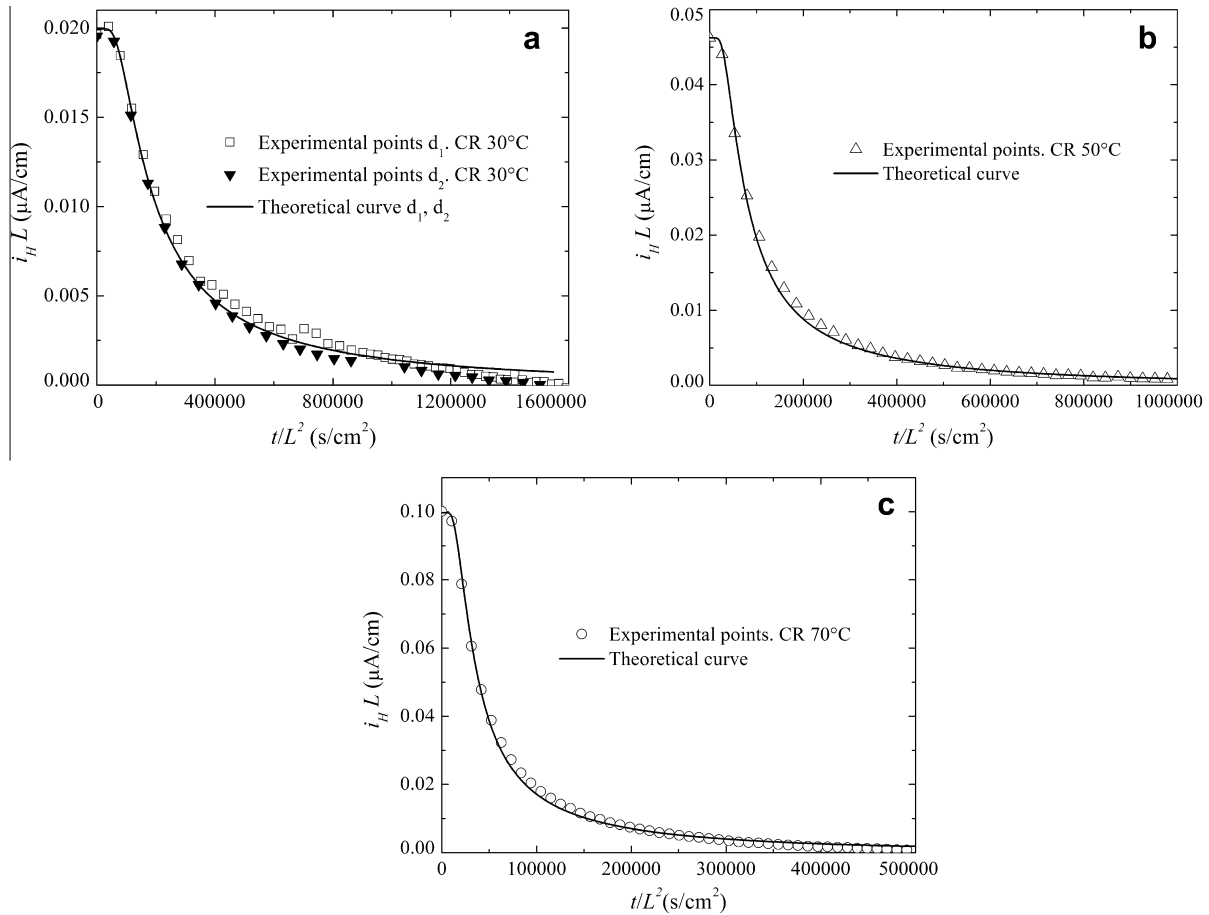
Fig. 4. Experimental points and theoretical curves of the decay transients the API 5L X60 steel in the cold-rolled (CR) condition: (a) 30 °C first transient (d_1) and second transient (d_2); (b) 50 °C; (c) 70 °C.

comparison. The literature values are either extrapolations of high temperature data [24] or from direct measurements at the temperature range of the present work [21,23]. The Φ values for the API 5L X60 steel were different and smaller than those for pure iron. The Φ/Φ_{Fe} ratios for both conditions were practically the same and independent of temperature, their value being about 0.67 when compared with references [21] and [23]. Contrarily, the Φ/Φ_{Fe} ratio

calculated using the high temperature data of Ref. [24] is close to unity. These results concerning the reduction Φ with increasing carbon content are consistent with those reported by Bruzzoni et al. [25] for a 1038 steel with 0.4%C in the states: quenched, quenched and tempered at 300, 550 and 650 °C, in the temperature range of 30–70 °C. The reported Φ values [25] were also lower than the Φ_{Fe} values. For the quenched material the Φ/Φ_{Fe} ratio was about 0.5 and it increased with tempering temperature up to a value of 0.8 for the tempering temperature of 650 °C.

3.4. Weak traps

The software used in this work to calculate the theoretical permeation transients considers an arbitrary D_{app} value that minimizes the error of the fit. The D_{app} parameter is an apparent diffusion coefficient, which is interpreted as that of a crystalline lattice containing weak traps. On the other hand, $D_L = 5.12 \times 10^{-4}$ exp $[(-4.15 \text{ kJ/mol})/RT] \text{ cm}^2 \text{ s}^{-1}$ [23] is the diffusion coefficient of a nearly perfect iron lattice, through which H diffuses without being trapped; then $D_{app} < D_L$. Weak traps are defined in the Appendix as that traps with trap occupancy θ_w negligible against unity. Weak traps are characterized by a low trap binding energy; the apparent diffusion coefficient D_{app} associated with the presence of weak traps is given by Eq. (A.8).

In the Appendix it is demonstrated that weak traps in iron and low alloy steels have a binding energy of $|\Delta G_w| < 35 \text{ kJ mol}^{-1}$. Consequently, the parameters ΔG and N reported in Tables 2 and 3 only give information on the strong traps; instead, weak traps

Fig. 5. Arrhenius type plot of the permeation coefficient Φ (mol H s^{-1} cm^{-1} bar$^{-1/2}$) of pure iron (literature references) and of the API 5L X60 in the as-received (AR) and cold-rolled (CR) conditions (present work).

are implicitly considered in the value of D_{app}. Eq. (A.8) allows to obtain the product $N_w \times K_w$ from D_{app}, but it is not possible to asses individual values of N_w and K_w. Therefore, in order to characterize the weak traps in the API 5L X60 steel it is necessary to analyze the dependence of D_{app} with temperature. From Eq. (A.8) the following expression is obtained:

$$\ln K_w = \ln\left(\frac{D_L}{D_{app}} - 1\right) + \ln N_w \qquad (3)$$

In Fig. 6, $(D_L/D_{app} - 1)$ is plotted in an Arrhenius type plot, where the D_{app} values are those taken from Tables 2 and 3 and correspond to the API 5L X60 steel in the AR and CR conditions, respectively. The slope of the plot in Fig. 6 is related to the trapping enthalpy ΔH_w by the thermodynamic relation:

$$\frac{d \ln K_w}{dT} = \frac{\Delta H_w}{RT^2} \qquad (4)$$

A linear fit of the data represented in Fig. 6 yields $\Delta H_w = -(36 \pm 4)\,\mathrm{kJ\,mol^{-1}}$ for the AR condition and $\Delta H_w = -(29.3 \pm 0.3)\,\mathrm{kJ\,mol^{-1}}$ for the CR condition. Assuming as a first approach that the trapping entropy is negligible, then it can be considered that $\Delta G_w \approx \Delta H_w$. The densities of the weak traps are obtained from the y-intercept of the plot: $N_w = 1.4 \times 10^{-5}\,\mathrm{mol/cm^3}$ for the AR state and $N_w = 7.9 \times 10^{-4}\,\mathrm{mol/cm^3}$ for the CR state. The ΔG_w value for the CR condition is within the theoretical interval $|\Delta G_w| < 35\,\mathrm{kJ\,mol^{-1}}$ established in the Appendix; however the ΔG_w value for the AR condition slightly exceeds this limit. The comparison between the two conditions of the API 5L X60 steel shows that N_w is ca. 60 times higher in the CR state than in the AR state.

3.5. Hydrogen traps and microstructure

In this section different microstructural defects in the API 5L X60 steel are considered as possible candidates for H trapping sites. An attempt is made of estimating the trap densities corresponding to each defect.

The first defect to consider is a dislocation. For quenched and tempered steels, dislocation densities have been measured using X-ray diffraction and transmission electron microscopy [26,27]; the measured values ranged from 10^9 to $4 \times 10^{10}\,\mathrm{cm^{-2}}$. Assuming one trapping site per dislocation plane and dislocation planes separated by $a/\sqrt{2}$ where a is the lattice parameter of bcc iron, a trap density ranging from 0.08×10^{-6} to $3 \times 10^{-6}\,\mathrm{mol\,cm^{-3}}$ is esti-

Fig. 6. Arrhenius type plot to evaluate the free energy and density of the weak traps. API 5L X60 steel in the as-received (AR) and cold-rolled (CR) conditions.

mated for the AR condition. As a rough approximation it can be considered that this figure is increased up to one order of magnitude in the CR condition with 2% plastic strain.

Other possible traps are the ferrite–cementite and ferrite–inclusion interfaces. The ferrite–inclusion interfaces are not considered in the present work since the inclusion content of this steel is very low. The trapping capacity of the ferrite–cementite interfaces can be roughly estimated assuming that: (1) the cementite particles are spheres of ca. 0.3 μm diameter; (2) the carbon content of the ferrite is negligible, thus practically all carbon is precipitated as cementite; (3) the H atoms occupy hollow sites on the {111} ferrite plane with a trap site area of a^2. This calculation yields a trap density of $9 \times 10^{-6}\,\mathrm{mol\,cm^{-3}}$.

The trap density related to trap boundaries has been estimated from the average grain size of the API 5L X60 steel (ca. 4 μm) with the simple assumption that the grains are closely packed cubes and the area of the trap site is a^2 as stated above. The resulting trap density is $1.5 \times 10^{-5}\,\mathrm{mol\,cm^{-3}}$.

The density of weak traps N_w is markedly high in both the AR and CR conditions, i.e. 1.45×10^{-5} and $7.9 \times 10^{-3}\,\mathrm{mol\,cm^{-3}}$ respectively. The estimated trap density for grain boundary sites agrees well with the trap density observed in the as-received state, while the estimated ferrite–cementite and dislocation trap densities are lower than the observed value. As a first approximation it can be stated these three defects (dislocation, ferrite–carbide interfaces and grain boundaries) are not excluded as possible weak trap sites in the AR material. Some trapping energies reported in the literature are $27.2\,\mathrm{kJ\,mol^{-1}}$ for dislocations [11], $26.8\,\mathrm{kJ\,mol^{-1}}$ for ferrite–carbide interfaces [28] and $9.6\,\mathrm{kJ\,mol^{-1}}$ for grain boundaries [13]. These energies lie within the range corresponding to weak traps as defined in the present work.

Concerning the CR condition, the assignment of the weak traps to a particular microstructural defect seems difficult. The observed trap density largely exceeds the estimated trap density for ferrite–carbide interfaces and grain boundaries (it is assumed that ~2% plastic strain does not influence either ferrite–carbide or grain boundary areas). With respect to dislocations, the plastic strain is expected to cause an increase in dislocation density. For example, assuming a dislocation density of $\sim 4 \times 10^9\,\mathrm{cm^{-2}}$ for the CR state, i.e. one order of magnitude higher than for the AR condition, the estimated trap density would be $3 \times 10^{-5}\,\mathrm{mol/cm^3}$. However, this value is still more than two orders of magnitude lower than the weak trap density determined in the present work for the API 5L X60 in the CR condition. Thus, it is difficult to associate the weak traps of this condition to any particular microstructural defect. It appears that weak traps are more likely associated to stress fields around dislocations or around second phase particles, developed during the process of plastic deformation. Kumnick and Johnson [11] and other researchers noted that the majority of the trapping sites caused by plastic deformation of iron were eliminated by thermal treatment at temperatures at which the dislocations were stable. This observation is in agreement with the hypothesis proposed above.

Concerning the high energy or "strong" traps, three types are identified in the present work. The first type has a trapping energy of ca. 58–$60\,\mathrm{kJ\,mol^{-1}}$ and is present both in the AR and CR conditions, with densities of 8×10^{-9} and $1 \times 10^{-7}\,\mathrm{mol\,cm^{-3}}$ respectively. The second and third types are only present in the CR condition. The second type has a trapping energy of 64–$71\,\mathrm{kJ\,mol^{-1}}$ and a trap density of $\sim 2 \times 10^{-8}\,\mathrm{mol\,cm^{-3}}$. The third type is a strong trap of higher energy that is emptied in the oven degassed state. The corresponding trapping energy and density are roughly estimated from Table 3 as $>76\,\mathrm{kJ\,mol^{-1}}$ and $\sim 1 \times 10^{-8}\,\mathrm{mol\,cm^{-3}}$ respectively.

The strong traps present in the AR condition should not be associated with plastic strain but with some microstructural feature.
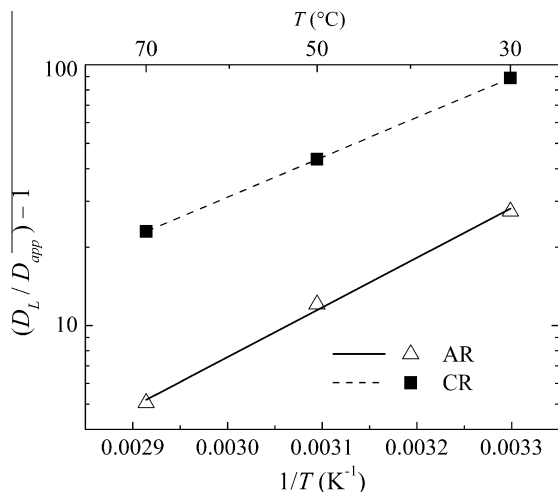
Any hypothesis would be highly speculative; only is worth noting that Nb and Ti are micro alloying elements of the present API 5L X60 steel (Table 1). It has been reported that coherent or semi coherent Nb and Ti carbides can act as strong trapping sites for hydrogen [29].

The strong traps present in the CR condition may be associated with plastic strain. The overall value of strong trap density (type1 + type 2 + type 3) is $\sim 1.3 \times 10^{-7}$ mol cm^{-3}. This value is more than two orders of magnitude lower than the trap density of 3×10^{-5} mol/cm^3 linked to the dislocation cores estimated above. Then, it is difficult to assign strong taps to dislocation cores by reasons both of trap density and trap energy values. This observation suggests that either not all dislocation cores are available to hydrogen, or that some of the observed high energy traps might be associated with special defects with higher energy than ordinary dislocation cores. Kumnick and Johnson [11] observed deep trapping sites with densities ranging from 0.8×10^{-7} to 3×10^{-7} mol cm^{-3} and trapping energy of ~ 59 kJ mol^{-1} for cold-rolled iron with 15–80% reduction in thickness. These low trap density values were attributed to "heterogeneous sites along dislocation cores, presumably jogs or multiple jogs, or with the point defect debris left behind by the jogs of dislocations moving during plastic deformation" rather than normal dislocation cores. Presumably these high energy sites are not eliminated by annealing. Other possible high energy traps, as mentioned in the introduction, are microvoids or microcracks [10,13,16], and vacancy aggregates [14].

The analysis carried out in the present work reveals a clear relationship between the degree of plastic strain and the density of both weak and high energy traps in the API 5L X60 steel. It should be pointed out that the hypotheses proposed above concerning the nature of the different trap types are highly speculative. The unambiguous assignment of microstructural defects to the different types of traps found in the API 5L X60 steel is beyond its scope of the present work.

4. Conclusions

1. Hydrogen traps in the API 5L X60 steel, and by extension in iron and low alloy steels, can be classified as strong or weak according to whether they change the shape of the permeation transient or not.
2. Diffusion and trapping parameters of the API 5L X60 steel were obtained from the fit calculated permeations transients to experimental ones. These parameters are the apparent diffusion coefficient Dapp, which contains the information on the weak traps, and the trap density N and the free energy of trapping ΔG of the strong traps. The calculated permeation transients were obtained using a model of saturable traps in local equilibrium.
3. A large density of low energy traps (weak traps) is observed in the API 5L X60 steel in both the as-received (AR) and the cold-rolled with 2.1 ± 0.3% reduction in thickness (CR) conditions.
4. The API 5L X60 steel in the AR condition presents weak traps with $N = 1.5 \times 10^{-5}$ mol cm^{-3} and $\Delta G = -(36 \pm 4)$ kJ mol^{-1} and strong traps with $N = 0.8 \times 10^{-8}$ mol cm^{-3} and $\Delta G = -(58.3 \pm 0.3)$ kJ mol^{-1}.
5. The API 5L X60 steel in the CR condition shows a notable increase of more than one order of magnitude in the trap density with respect to the AR condition. This increase is observed either for weak or strong traps.
6. After cold-working weak trap parameters are $N = 7.9 \times 10^{-4}$ mol cm^{-3} and $\Delta G = -(29.3 \pm 0.3)$ kJ mol^{-1}. Strong traps of three different types are detected with an overall density $N = 1.3 \times 10^{-7}$ mol cm^{-3} and ΔG ranging from -57 to -76 kJ mol^{-1}.

Appendix

A.1. Theoretical considerations

The present computer simulation of the hydrogen permeation transients is based on the model of McNabb and Foster [17] of saturable hydrogen traps with simple kinetic laws for trapping and detrapping. In the present article, the notation used by McNabb and Foster is partly changed. Assuming only one type of trap and unidirectional diffusion, the differential equation to solve is:

$$\frac{\partial c_L}{\partial t} + k_T c_L (1 - \theta) N - p\theta N = D_L \frac{\partial^2 c_L}{\partial x^2} \tag{A.1}$$

where c_L is the lattice H concentration, i.e. the concentration of H in normal interstitial lattice sites (NILS), t is time, D_L is the lattice diffusion coefficient, x is the spatial coordinate, N is the trap density, θ is the fraction of occupied traps and k_T and p are the trapping and detrapping kinetic constants, respectively. Eq. (A.1) can be rewritten in terms of dimensionless variables:

$$X = x/L; \quad u = c_L/c_{L0}; \quad \tau = D_L t/L^2; \quad w = N\theta/c_{L0} \tag{A.2}$$

where L and c_{L0} are a characteristic dimension and a characteristic lattice H concentration of the system respectively. For the present case of H permeation through a metallic membrane, L is the membrane thickness and c_{L0} is the lattice H concentration beneath the entry surface of the permeation membrane:

$$\frac{\partial u}{\partial \tau} + \frac{NL^2}{D_L} k_T u - \frac{L^2 p}{D_L} w - \frac{c_{L0} L^2 k_T}{D_L} uw = \frac{\partial^2 u}{\partial X^2} \tag{A.3}$$

or, by defining the constants λ, μ, and ν:

$$\frac{\partial u}{\partial \tau} + \lambda u - \mu w - \nu uw = \frac{\partial^2 u}{\partial X^2}, \quad \lambda = \frac{NL^2 k_T}{D_L} \quad \mu = \frac{L^2 p}{D_L} \quad \nu = \frac{c_{L0} L^2 k_T}{D_L} \tag{A.4}$$

The hypothesis of local equilibrium proposed by Oriani [16] assumed here. This hypothesis implies that the detrapping time constant $(1/p)$ is much lower than the diffusion time constant (L^2/D_L). As reported in the next paragraphs, in the present work has been empirically found that the choice of $1/p \leqslant 0.001 \, L^2/D_L$ (i.e. $\mu \geqslant 1000$) usually guarantees local equilibrium.

With the assumption of local equilibrium, the fraction of occupied tramps (θ) is a function only of the lattice hydrogen concentration (c_L):

$$\theta = \frac{Kc_L}{1 + Kc_L}; \quad K = \frac{k_T}{p} \tag{A.5}$$

where K is the equilibrium constant of the trapping reaction. The resulting differential equation is

$$\frac{\partial c_L}{\partial t} + N \frac{\partial}{\partial t} \left(\frac{Kc_L}{1 + Kc_L} \right) = D_L \frac{\partial^2 c_L}{\partial x^2} \tag{A.6}$$

If $Kc_L \ll 1$ (weak traps, defined as those with $\theta \ll 1$), then Eq. (A.6) is simplified and can be analytically solved. The solution for the H flux J_H [mol H/(cm^2 s)] of the permeation buildup transient is:

$$J_H = \frac{D_{app} c_0}{L} \left(1 + 2 \sum_{n=1}^{\infty} (-1)^n \exp \left(-n^2 \pi^2 \frac{D_{app} t}{L^2} \right) \right) \tag{A.7}$$

where the symbol c is introduced to denote the H concentration of hydrogen located either in NILS or in weak trap sites as defined in Eq. (A.8); c_0 specifies the concentration c at a location just beneath the input surface of the permeation membrane. D_{app} is the apparent diffusion coefficient which is also defined in Eq. (A.8):

$$c = c_L + c_W = c_L(1 + K_W N_W); D_{app} = \frac{D_L}{1 + K_W N_W} \tag{A.8}$$

The sub-index W in Eq. (A.8) is used to denote "weak" traps. According to [16], $c = c_L (1 + K_W N_W)$. Particularly at the entry surface $c_0 = c_{L0} (1 + K_W N_W)$.

Eq. (A.7) shows that the weak traps do not cause a distortion in the shape of the permeation transient but just a change in the time scale with respect to a trap free material with $D_{app} = D_L$. It is worth noting that, according to Eq. (A.8), different combinations of $K_W N_W$ would yield the same value of D_{app}, and consequently would produce indistinguishable permeation transients. This means that a single permeation transient does not allow assessing individual values of weak trap density and weak trap energy. The present treatment is developed in such way that the effect of the weak traps is only reflected in the value of D_{app}. In the presence of strong traps (θ not negligible against unity), Eq. (A.6) has no analytical solution but must be solved by a numerical method. Before dealing with the numerical method itself, Eq. (A.6) is modified by taking into account that, according to Eq. (A.7), the ensemble of lattice and weak traps behaves as a simple diffusion system. Then, Eq. (A.6) is rewritten in terms of D_{app}, c, the density of strong traps (N_S) and the equilibrium constant for the trapping reaction of the strong traps K_S:

$$\frac{\partial c}{\partial t} + N_S \frac{\partial}{\partial t}\left(\frac{K_S c_L}{1 + K_S c_L}\right) = D_{app} \frac{\partial^2 c}{\partial x^2} \tag{A.9}$$

In the above equation the effect of the weak trap density and energy is implicitly reflected in the value of D_{app}. Then, the only traps to be considered explicitly are the strong traps. Eq. (A.9) expresses the central idea of the present method, which is the use of D_{app} instead of D_L and concentrates on the strong traps which are the ones that change the shape of the permeation transient.

Now, according to Eq. (A.8), the lattice concentration c_L is expressed in terms of c:

$$\frac{\partial c}{\partial t} + N_S \frac{\partial}{\partial t}\left(\frac{K'c}{1 + K'c}\right) = D_{app} \frac{\partial^2 c}{\partial x^2} \tag{A.10}$$

where

$$K' = \frac{K_S}{1 + K_W N_W} \tag{A.11}$$

The constant K' in Eq. (A.10) is related to K_S by Eq. (A.11). K_S is the true equilibrium constant which uses the lattice hydrogen concentration as the reference state. The numerical methods to solve the McNabb and Foster's equations presented previously (Thomas and Stern [18], Johnson and Lin [15], Ferriss et al. [30], Ramunni et al. [19], use the lattice diffusion coefficient D_L. The present approach uses, instead of D_L, an apparent diffusion coefficient D_{app} which contains the effect of the weak traps. The advantages of this method are: (1) the focus is on the strong traps, about which the shape of the permeation transient contains valuable information; (2) D_{app} may be orders of magnitude lower than D_L; therefore, the calculation speed is improved since the time steps are inversely proportional to the diffusion coefficient as it is shown below.

A.2. Numerical method

To solve the differential Eq. (A.10) a finite difference method is used. The permeation membrane is divided in m slices or volume elements of thickness L/m. Each volume element is identified by an index j ($1 \leqslant j \leqslant m$). The extreme values $j = 1$ and $j = m$ correspond to volume elements adjacent to the entry and exit side of the permeation membrane, respectively. The diffusion path is L/m between adjacent slices and $L/2m$ for the entry and exit interfaces. The diffusion into the volume element is described by the right hand member of Eq. (A.10).

The overall H concentration (c_T) is defined as the sum of lattice, weakly trapped and strongly trapped hydrogen concentrations: $c_T = c_L + c_W + c_S = c + c_S$.

The numerical calculation proceeds from an initial condition in a succession of cycles. Each cycle is composed of two steps. The first step of the method is to calculate Δc_{Tj}, which is defined as the increase of the overall H concentration in each volume element (j) by diffusion during a time interval (Δt). Δc_{Tj}, is calculated *via* the right-hand member of Eq. (A.10), where the second order partial derivatives are approximated by finite increments, taking into account the different diffusion paths:

$$\Delta c_{Tj} = D_{app} \frac{\partial^2 c}{\partial x^2} \Delta t$$

$$\frac{\partial^2 c}{\partial x^2} \approx \frac{2c_0 + c_2 - 3c_1}{(L/m)^2} \quad (j = 1)$$

$$\frac{\partial^2 c}{\partial x^2} \approx \frac{c_{j-1} + c_{j+1} - 2c_j}{(L/m)^2} \quad (1 < j < m) \tag{A.12}$$

$$\frac{\partial^2 c}{\partial x^2} \approx \frac{2c_{m+1} + c_{m-1} - 3c_m}{(L/m)^2} \quad (j = m)$$

The second step is to achieve simultaneously the mass conservation and local equilibrium condition within each volume element. For only one type of strong traps, the following quadratic equation must be solved for c_{new}:

$$c_{old} + \frac{N_S K' c_{old}}{1 + K' c_{old}} + \Delta c_T = c_{new} + \frac{N_S K' c_{new}}{1 + K' c_{new}} \tag{A.13}$$

where the sub-indexes "*old*" and "*new*" refer to the values of c before and after the time interval Δt has elapsed. Once c_{new} is calculated for each volume element, the H flux at the exit side of the permeation membrane J_H is calculated with Fick's law:

$$J_H = -D_{app} \frac{\partial c}{\partial x}(x = L) \approx D_{app} \frac{c_j - c_{j+1}}{\frac{L}{2m}} \tag{A.14}$$

A usual technique to detect H at the exit side of the permeation membrane is the electrochemical method. In this method, the measured hydrogen current density i_H is related to J_H by the Faraday's constant F:

$$i_H = \frac{J_H}{F} \tag{A.15}$$

provided that H concentration is expressed as mol H per unit volume.

After carrying out the former procedures, the time is increased in Δt and the cycle is repeated from the first step. The successive values of i_H as a function of time constitute the "calculated" or "simulated" permeation transient.

The time interval Δt is chosen sufficiently low in order to keep the system stable. For this kind of diffusion systems Δt is usually given by

$$\Delta_t = \frac{L^2}{D_{app} m^2} r \tag{A.16}$$

where r is the so called mesh ratio [18]. For the present system, $r \leqslant 0.2$ guarantees numerical stability. Taking into account Eq. (A.16), Eq. (A.12) can be rewritten as:

$$\Delta c_{Tj} \approx r(2c_0 + c_2 - 3c_1) \quad (j = 1)$$
$$\Delta c_{Tj} \approx r(c_{j-1} + c_{j+1} - 2c_j) \quad (1 < j < m) \tag{A.17}$$
$$\Delta c_{Tj} \approx r(2c_{m+1} + c_{m-1} - 3c_m) \quad (j = m)$$

The method described above considers only one type of strong traps. However, it can be easily generalized to many types of traps with densities N_{S1}, N_{S2}... and equilibrium constants K_{S1}, K_{S2}... by rewriting Eq. (A.13):

$$c_{old} + \frac{N_{S1}K'_1 c_{old}}{1 + K'_1 c_{old}} + \frac{N_{S2}K'_2 c_{old}}{1 + K'_2 c_{old}} + \cdots + \Delta c_T$$
$$= c_{new} + \frac{N_{S1}K'_1 c_{new}}{1 + K'_1 c_{new}} + \frac{N_{S2}K'_2 c_{new}}{1 + K'_2 c_{new}} + \cdots \tag{A.18}$$

In this case, Eq. (A.18) has no analytical solution and c_{new} is obtained by a numerical method such as the Newton–Raphson method.

For the present calculations, the values adopted for the mesh ratio and the number of volume elements were $r = 0.2$ and $m = 40$ respectively. The choice of $m = 40$ guarantees sufficient accuracy of the numerical solution.

A.3. The free energy of trapping

The free energy of trapping ΔG can be obtained from the thermodynamical relation:

$$\Delta G^0 = -RT \ln K \tag{A.19}$$

where R is the universal gas constant and T is the absolute temperature. ΔG^0 is the standard change of free energy for the trapping reaction. The reference state for hydrogen as solute in NILS is of the Henry's type (ideal dilute solution) with $c_L = 1$ mol cm^{-3}. The reference state for trapped hydrogen corresponds to a trap occupancy $\theta = 0.5$. In the rest of the present article, ΔG and "free energy of trapping" are used instead of ΔG^0 and "standard change of free energy for the trapping reaction" for the sake of simplicity. Activity coefficients are assumed to be unity throughout this article.

For the case of the strong traps, it is useful to express their free energy of trapping ΔG_S as a function of the parameters K' and D_{app} used for the calculation of the permeation transient as described above. This is accomplished by combining Eq. (A.8), (A.11), and (A.19):

$$\Delta G_S = \Delta G' - RT \ln \frac{D_L}{D_{app}} ; \Delta G' = -RT \ln K' \tag{A.20}$$

In fact, $\Delta G'$ is the parameter handled by the software. In order to obtain ΔG_S, $\Delta G'$ must be corrected according to Eq. (A.20).

A.4. Buildup and decay transients

The present method is able to calculate either buildup or decay permeation transients. This is achieved by choosing the appropriate initial and boundary conditions:

For the buildup transient the initial condition is $c_j = 0$ for $1 \leqslant j \leqslant m$ and the boundary conditions are: $c_j = c_0$ for $j = 0$ and $c_j = 0$ for $j = m + 1$.

For the decay transient the initial condition is $c_j = c_0$ $(m - j + 1/2)$ for $1 \leqslant j \leqslant m$ and the boundary conditions are: $c_j = 0$ for $j = 0$ and $c_j = 0$ for $j = m + 1$.

A.5. Fitting procedure

Besides calculating the permeation buildup or decay transient, the developed software allows the possibility to repeat the calcula-

tion with varied parameters in order to fit the calculated transient to experimental data. The initial list of parameters ($L, T, i_{Hss}, D_{app}, \Delta G_{S1}, K_{S1}, \Delta G_{S2}, K_{S2}$) is supplied by the user. The parameter i_{Hss} is the steady state hydrogen current density. All parameters of this list except L and T can be selected to vary. The software used in the present work admits as many as two types of strong traps. The fitting criterion is the minimization of the mean quadratic difference between calculated and experimental points, defined as:

$$Deviation = \frac{1}{i_{H,ss}} \sqrt{\frac{1}{n_{exp}} \sum_{k=1}^{n_{exp}} (i_{H,calc,k} - i_{H,exp,k})^2} \cdot 100\% \tag{A.21}$$

where n_{exp} is the number of experimental points; $i_{H,calc,j}$ and $i_{H,exp,j}$ are the calculated and experimental hydrogen current density, respectively.

A.6. Validation of the present method

Typical permeation transients calculated with the present method (which assumes local equilibrium) were also obtained by means of a software presented previously by Ramunni et al. [19]. This software does not assume local equilibrium and directly solves the McNabb and Foster's Eq. (A.4). The parameters λ, μ, and ν for the software of Ramunni et al. [19] were obtained through replacement of the parameters D_L, K and N in Eq. (A.4) and (A.5) by the present parameters D_{app}, K' and N_S and assuming an arbitrary value for μ. The coincidence of the permeation transients calculated by both methods was reached for values of μ higher than 1000. Then, it is considered that $\mu \geqslant 1000$ is a good criterion for the existence of local equilibrium.

A.7. Weak and strong traps

The concept of weak and strong traps has been defined only qualitatively in the former paragraphs. Then, a quantitative criterion to establish whether a trap is weak or strong has been investigated. For iron base alloys, it is expected that this criterion is essentially the value of the free energy of trapping ΔG, but also the temperature and the input hydrogen activity can play a secondary role. In the present work the effect of $|\Delta G|$ has been investigated.

The input hydrogen activity assumed here was that of typical gas phase charging experiments (hydrogen partial pressure = 0.1 MPa) and the temperature was that of typical electrochemical permeation
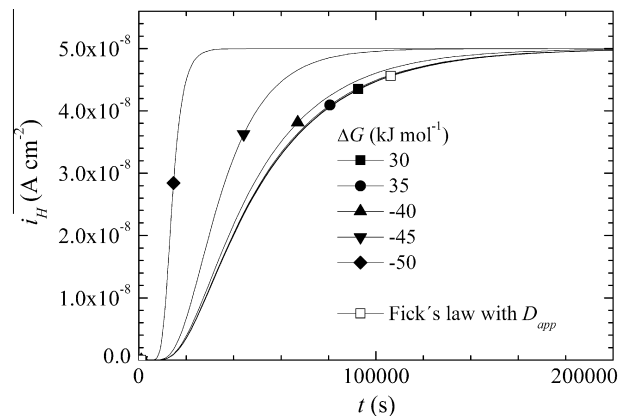
Fig. A1. Hydrogen permeation buildup transients simulated by a finite difference method to investigate the deviation from Oriani's Eq. (A.8). $L = 0.4$ cm; $D_L = 10^{-5}$ cm^2 s^{-1}; K $N = 20$; $i_{H,ss} = 5 \times 10^{-8}$ A cm^{-2}, $T = 303.15$ K. K was calculated from different free energies of trapping ΔG (filled symbols). The analytical solution of the Fick's law (Eq. (A.7)) using $D = D_{app}$ from Eq. (A.8) is also plotted (—□—).
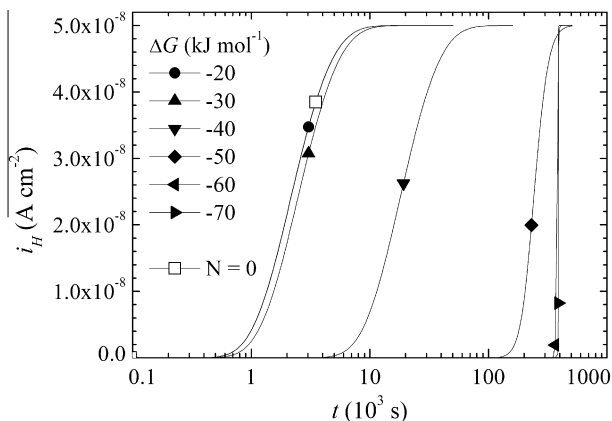
Fig. A2. Hydrogen permeation buildup transients simulated by a finite difference method. Effect of the free energy of trapping (ΔG). $L = 0.4$ cm; $D_L = 10^{-5}$ cm^2 s^{-1}; $N = 10^{-6}$ mol cm^{-3}; $i_{Hss} = 5 \times 10^{-8}$ A cm^{-2} and $T = 303.15$ K. $-\square-$: trap free lattice. Filled symbols: lattice with traps ($N = 10^{-6}$ mol cm^{-3}) with different values of ΔG.

experiments (303 K). The parameter i_{Hss} was obtained from the permeation coefficient of iron [8]. The assumed diffusion coefficient was 10^{-5} cm^2 s^{-1}, typical of a trap free material [23].

For a first series of runs ΔG was varied from -20 to -50 kJ mol^{-1}. The value of K was obtained with Eq. (A.19), and the value of N was chosen in order to keep the value of $K \times N$ fixed, *i.e.* $K \times N = 20$. The results of the calculations show that as ΔG is increased, the simulated permeation transients result indistinguishable, provided that $|\Delta G| \leqslant \sim 35$ kJ mol^{-1}. For $|\Delta G| > \sim 35$ kJ the permeation transients change: they develop in shorter times as $|\Delta G|$ increases as shown in Fig. A1. Then, traps with $|\Delta G| \leqslant \sim 35$ kJ mol^{-1} are considered as weak, and traps with $|\Delta G| > \sim 35$ kJ mol^{-1} are considered as strong.

A second series of runs was performed with a fixed value of $N = 10^{-6}$ mol cm^{-3} and ΔG ranging from -20 to -80 kJ mol^{-1}. The calculated permeation transients were plotted using a logarithmic time scale. As $|\Delta G|$ increases in the weak trap domain (up to ~ 35 kJ mol^{-1}) the plotted transients keep their shape but are shifted to the right (higher times). When $|\Delta G|$ increases beyond 35 kJ mol^{-1} the plotted transients continue being shifted to the right but become steeper. For $|\Delta G| > \sim 65$ kJ mol^{-1} the permeation transient looks similar to a step function as is shown in Fig. A2. The latter behavior is that of a diffusion front with trap occupancy $\theta \approx 1$ behind the front and $\theta \approx 0$ ahead of the front. The breakthrough time t_b is the time at which the diffusion front reaches the exit side. It can be shown that

$$t_b = \frac{N L F}{2 i_{H,ss}} \qquad (A.22)$$

In the present case, t_b calculated from Eq. (A.22) is 3.86×10^5 s and agrees very well with the location of the step. The second series of runs show that the maximum free energy of trapping that can be assessed by the analysis of a permeation curve in the reported conditions is ~ 65 kJ mol^{-1}.

Similar calculations performed at 343 K revealed $|\Delta G| \leqslant \sim 35$ kJ mol^{-1} for the "weak trap" behavior and $|\Delta G| > \sim 65$ kJ mol^{-1} for the "diffusion front" behavior. These critical values of $|\Delta G|$ are very similar to those obtained at 30 °C. It is expected that the critical values of $|\Delta G|$ will be slightly reduced as the hydrogen input activity increases.

A.8. Conclusions

The present method serves to analyze experimental hydrogen permeation buildup or decay transients *via* a least squares fitting procedure.

1. It is based on the McNabb and Foster's model of saturable traps with the Oriani's assumption of local equilibrium.
2. Domains of "weak trap", "strong trap" and strong trap with "diffusion front" behavior have been established for the present experimental conditions as a function of the free energy of trapping ΔG.
3. The effect of the weak traps is reflected in the value of the apparent diffusion coefficient D_{app}, which is obtained as a fitting parameter.
4. Strong traps are characterized by a trap density N and a free energy of trapping ΔG. N is directly obtained as a fitting parameter; ΔG is obtained from the fitting parameter $\Delta \acute{G}$ by an equation that takes into account the change of the reference state implied by the use D_{app} instead of D_L.
5. In the "diffusion front" domain, N can be accurately determined but not ΔG.
6. In the present work, up to two different types of traps have been be characterized. However, the developed method allows to increase that number if necessary.

References

[1] T. Llewellyn, R.C. Hudd, Steels: Metallurgy and Applications, third ed., Butterworth, Heinemann, Oxford, 1998.
[2] C.D. Beachem, A new model for hydrogen assisted cracking (Hydrogen Embrittlement), Metall. Trans. A. 3 (1972) 437–451.
[3] R.P. Gangloff, R.P. Wei, Gaseous Hydrogen Embrittlement of high strength steels, Metall. Trans. A. 8 (1977) 1043–1053.
[4] G.M. Pressouyre, Trap theory of Hydrogen Embrittlement, Acta Metall. 28 (1980) 895–911.
[5] R.P. Gangloff, Critical Issues in Hydrogen Assisted Cracking of Structural Alloys, in: Sergei Shipilov (Eds.), Environment Induced Cracking of Metals (EICM 2), Elsevier Science, Oxford, in press 2006.
[6] L.S. Darken, R.P. Smith, Behavior of hydrogen in steel during, after immersion in acid, Corros 5 (1949) 1.
[7] U.V. Bath, H.K. Lloyd, Effect of cold-work on hydrogen in steel, J. Iron Steel Inst. 165 (1950) 382–389.
[8] E. Riecke, Untersuchungen zum Eifluß des Stahlgefüges auf die stationäre Wasserstofpermeation, Werkst. Korros. 32 (1981) 66–72.
[9] J.H. Keeler, H.M. Davis, Density and hydrogen occlusion of some ferrous metals, J. Met. Trans. AIME (1953) 44–48.
[10] A.J. Kumnick, H.H. Johnson, Hydrogen transport through annealed and deformed Armco iron, Metall. Trans. 5 (1974) 1199–1206.
[11] A.J. Kumnick, H.H. Johnson, Deep trapping states for hydrogen in deformed iron, Acta Metall. 28 (1980) 33–39.
[12] R.S. Chaudhary, E. Riecke, Untersuchungen zum Eifluß des Stahlgefüges auf die instationäre Wasserstofpermeation, Werkst. Korros. 32 (1981) 73–78.
[13] W.Y. Choo, J.Y. Lee, Thermal analysis of trapped hydrogen in pure iron, Metall. Trans. 13A (1982) 135–140.
[14] M. Nagumo, K. Takai, N. Okuda, Nature of hydrogen trapping sites in steels induced by plastic deformation, J. Alloy. Compd. 293–295 (1999) 310–316.
[15] H.H. Johnson, R.W. Lin, Hydrogen and deuterium trapping in iron, in: I.M. Bernstein, A.W. Thompson (Eds.), Hydrogen Effects in Metals, Metallurgical Society AIME, New York, 1981, pp. 3–25.
[16] R.A. Oriani, The diffusion and trapping of hydrogen in steel, Acta Metall. 18 (1970) 147–157.
[17] A. McNabb, P.K. Foster, A new analysis of the diffusion of hydrogen in iron and ferritic steels, Trans. Metall. Soc. AIME 227 (1963) 618–626.
[18] P.G. Thomas, E.J. Stern, Efficient numerical modeling of hydrogen diffusion with trapping, J. Mater. Sci. 16 (1981) 3122–3130.
[19] V.P. Ramunni, T.D.P. Coelho, P.E.V. de Miranda, Interaction of hydrogen with the microstructure of low carbon steel, Mater. Sci. Eng A (2006) 504–514.
[20] P. Castaño Rivera, P. Bruzzoni, Interacción hidrógeno metal en un acero para gasoductos, Memorias Tercer Congreso Nacional y Segundo Congreso Iberoamericano de Hidrógeno y Fuentes Sustentables de Energía (2009).
[21] A.J. Kumnick, H.H. Johnson, Steady state hydrogen transport through zone refined irons, Metall. Trans. 6A (1975) 1087–1091.
[22] M.A.V. Devanathan, Z. Stachurski, The absorption and diffusion of electrolytic hydrogen in palladium, Proc. Roy. Soc. A 270 (1962) 90–102.
[23] E. Riecke, K. Bohnenkamp, Über den Einfluβ von Gitterstörstellen in Eisen auf die Wasserstoffdiffusion, Zeitschrift für Metallkunde 75 (1984) 76–81.
[24] R.F. Miller, J.B. Hudson, G.S. Ansell, Permeation of hydrogen through alpha iron, Metall. Trans. 6A (1975) 117–121.
[25] P. Bruzzoni, G. Domizzi, M.I. Luppo, D. Zalcman, J. Ovejero, Effect of Boron as a micro-alloying element on the behaviour of a 1038 steel in a hydrogen

environment, in: A.W. Thompson, N.R. Moody (Eds.), Hydrogen effects in materials The Minerals Metals and Materials Society (TMS), Warrendale, Pennsylvania, 1996, pp. 1001–1009.

[26] S. Takebayashl, T. Kunieda, N. Yoshinaga, K. Ushioda, S. Ogata, ISIJ Int. 50 (2010) 875–882.

[27] S.J. Pešiča, R. Kužel, A. Dronhofer, G. Eggeler, The evolution of dislocation density during heat treatment and creep of tempered martensite ferrite steels, Acta Mater. 51 (2003) 4847–4862.

[28] W.M. Robertson, A.W. Thompson, Permeation measurements of hydrogen trapping in 1045 steel, Metall. Trans. 11A (1980) 553–557.

[29] F.-G. Wei, T. Hara, K. Tsuzaki, Nano-precipitates design with hydrogen trapping character in high strength steels, in: Brian Somerday, Petros Sofronis, Russell Jones (Eds.), Effects of Hydrogen on Materials, Proceedings of the 2008 International Hydrogen Conference, ASM Int., 2009, pp. 448–455.

[30] D.H. Ferris, A. Turnbull, Analysis of reversible and irreversible hydrogen trapping in metals, NPL Report DMA (A) (1988) 154.